NaCl induced corrosion of Ti-6Al-4V alloy at high temperature

Clément Ciszak[a,*], Ioana Popa[a], Jean-Michel Brossard[b], Daniel Monceau[c], Sébastien Chevalier[a]

[a] ICB, UMR 6303CNRS-Université de Bourgogne, 21078 Dijon Cedex, France
[b] Veolia Recherche et Innovation, Zone portuaire de Limay, 291 Avenue Dreyfous-Ducas, 78520 Limay, France
[c] CIRIMAT-ENCIACET, UMR CNRS 5085, 31030 Toulouse, France

A B S T R A C T

This paper presents a study on the Ti-6Al-4V behaviour in presence of NaCl deposit under dry and moist air environments at 560 °C. The results evidence a detrimental effect of the NaCl deposit with a synergistic effect in presence of moist air environment. Treatments under dry and moist air with NaCl deposit for 600 h, lead respectively to weight gains per unit area 5 and 15 times higher than observed under classic oxidation in dry air. Enhancement of the corrosion phenomenon is attributed to the presence of gaseous metal chlorides, leading to the establishment of an active corrosion process.

Keywords:
A. Titanium
A. Alloy
B. SEM
B. X-ray diffraction
C. High temperature corrosion

1. Introduction

Ti-based alloys have been increasingly used in various domains such as chemical industry, medical engineering and aerospace for their high corrosion resistance, bio-compatibility, high specific strength and low-density. Their major asset in high temperature applications is the presence of addition elements, such as aluminium, which enhance their oxidation behaviour. This beneficial effect towards oxidation resistance is mainly due to the formation of alumina Al_2O_3 in the external part of the rutile layer [1–4].

Nevertheless, oxygen can diffuse deep inside the metallic substrate to form an oxygen dissolution area, which leads to embrittlement of the affected area [3,5,6]. Oxygen dissolution in the Ti matrix explains the gradual increase of the material hardness when approaching the metal-oxide interface. Various studies evaluated the depth of the oxygen dissolution area; they show that the oxygen dissolution is dependent on both temperature and time (for instance, the oxygen dissolution area is 10 μm deep after 70 h at 600 °C [3], but is deeper than 15 μm after only 3 h at 750 °C [6]).

Titanium alloys are sometimes asked to work beyond their original limits, especially in terms of thermal stresses, revealing uncertainties about their behaviour at high temperature (typically above 400 °C for the Ti-6Al-4V alloy). Another parameter that can influence significantly the material behaviour is the gaseous environment, especially the humidity. The material may even, in some cases, come in contact with species such as silica, sea salt or sulphates.

Humidity influences the oxidation mechanisms of the Ti-6Al-4V alloy, as in moist air, the corrosion scale is formed of two layers of rutile TiO_2, separated by an alumina rich area [7]. These three layers generally contain many defects such as pores and/or whiskers for the outer part [6], which are typical of the water vapour presence [8]. This difference in morphology would therefore suppose the existence of different oxidation mechanisms and oxygen dissolution depth under moist air oxidation. In fact, Pérez [9] showed that after being treated at 700 °C for 150 h, samples of pure titanium exposed to laboratory air and moist air present an oxide layer of 15 μm and 17 μm thick respectively. The oxygen dissolution area thickness enlarges from 30 μm to 40 μm. This larger oxygen dissolution depth could be attributed to the faster diffusion of OH^- ions compared to O^{2-} ions (because of their smaller size and lower charge), the hydroxyl ions coming from the adsorption and the dissociation of the water molecules at the oxide/atmosphere interface [10]. Other results are however more contrasted. Motte et al. [7] reported higher weight gain per unit area whereas Champin et al. [11] reported lower weight gain per unit area after treatment in moist air compared with dry air treatment. It is moreover mentioned that the oxidation kinetic is parabolic at the beginning of the oxidation [6,8], tending to a sub-parabolic regime for long duration treatments [8].

* Corresponding author.
E-mail address: clement.ciszak@u-bourgogne.fr (C. Ciszak).

http://dx.doi.org/10.1016/j.corsci.2016.04.016

Moreover, as it was described by Grabke et al. for low and high alloyed steels [12] and by Kawahara for a Ni-based alloy [13], corrosion phenomena can be more aggressive if salt crystals condensate on the material. This corrosion phenomenon generally involving solid or liquid mixed environments of NaCl and Na_2SO_4 is called "hot corrosion" [14–16]. Disastrous effects can occur at operating temperatures higher than the melting point of the mixture, what is defined as the type I of hot corrosion [14–16]. The effect appears to be more moderate below this temperature, defining the type II of hot corrosion [14–17], although just as harmful for the material. In his Ph.D. work, Tsaur [17] have also demonstrated that enhanced corrosion phenomenon can occur even if only solid NaCl is present. Very few studies on titanium alloys were done in these particular conditions. They showed parabolic oxidation kinetics 6 times larger than those observed in dry air, for a titanium alloy IMI 685 [18]. The observed corrosion layer is then porous, cracked and non-adherent to the metallic substrate. The oxide scale is rather dense in the inner part and rather porous in the outer part [18]. Both are composed of similar species to those observed after dry air treatment, namely: TiO_2 (rutile [18,19] and anatase [19]) phases optionally containing alloying elements [19], Al_2O_3 in the case of the Ti 6242 alloy [20] and sometimes the bi-component Na_2O, $5TiO_2$ [18]. Concerning the formation of these compounds, the same studies presume an inward diffusion of oxygen [18–20] and Cl^- [18,19] anions, concomitant with an outward diffusion of the metallic cations from the substrate [18] (increased by the presence of pores and cracks [19]). These hypotheses are often accompanied by assumptions of reactional mechanisms [19], which are thermodynamically consistent [20], but not demonstrated experimentally. They are systematically based on volatile chlorine species, which lead to the formation of TiO_2 rutile and in a particular case, to a mixed oxide $Na_xTi_yO_z$ as observed by Gurrappa [21], accompanied by a release of gaseous Cl_2 (which could justify the presence of blisters and pores). Furthermore, the dissolution phenomenon also appears to be strongly influenced by the presence of salts on the material surface, an oxygen dissolution area of about 500 μm deep has been observed after a treatment at 600 °C for 65 h in presence of molten salts mixture (90% Na_2SO_4, 10% NaCl) [21].

The few studies combining the two previous exposition conditions (moist air and NaCl deposit) report an increase of the weight gain per unit area of the samples (for Ti-6Al-4V [22] and Ti60 [23,24] alloys), up to a factor of 100 for an IMI 685 Ti-based alloy [18]. The morphology of the formed corrosion products is also affected by high porosity and roughness. High weight gains per unit area (compared to those observed after dry air treatment) are justified by an approach of the oxidation mechanisms combining the two previous approaches. Dissociation of water molecules in H^+ and OH^- would take place on defects present on the TiO_2 layer surface [24]. Concerning the reaction between the metallic substrate with NaCl and H_2O, it would result in the formation of titanium oxide TiO_2 [18,22–24], a mixed sodium-titanium oxide Na_2TiO_3 [22–24] and the release of gaseous di-hydrogen [22,23] and hydrochloric acid [22–24].

The objective of the present study is to better understand the influence of the NaCl deposit on the oxidation behaviour at high temperature (500 °C, 560 °C and 625 °C) of a largely used Ti alloy, Ti-6Al-4V, in both dry air and moist air conditions. In this purpose, four environments were considered: laboratory air, moist air, laboratory air with NaCl deposit and moist air with NaCl deposit. Several preliminary tests were performed at the 3 temperatures mentioned above; however this paper focuses on the intermediate temperature of 560 °C.

Corrosion products were analysed by means of X-rays diffraction (XRD) and scanning electron microscopy (SEM) coupled to energy dispersive X-ray (EDS) analysis, while the oxygen dissolution area was identified through hardness measurements done over the whole thickness of the metallic material.

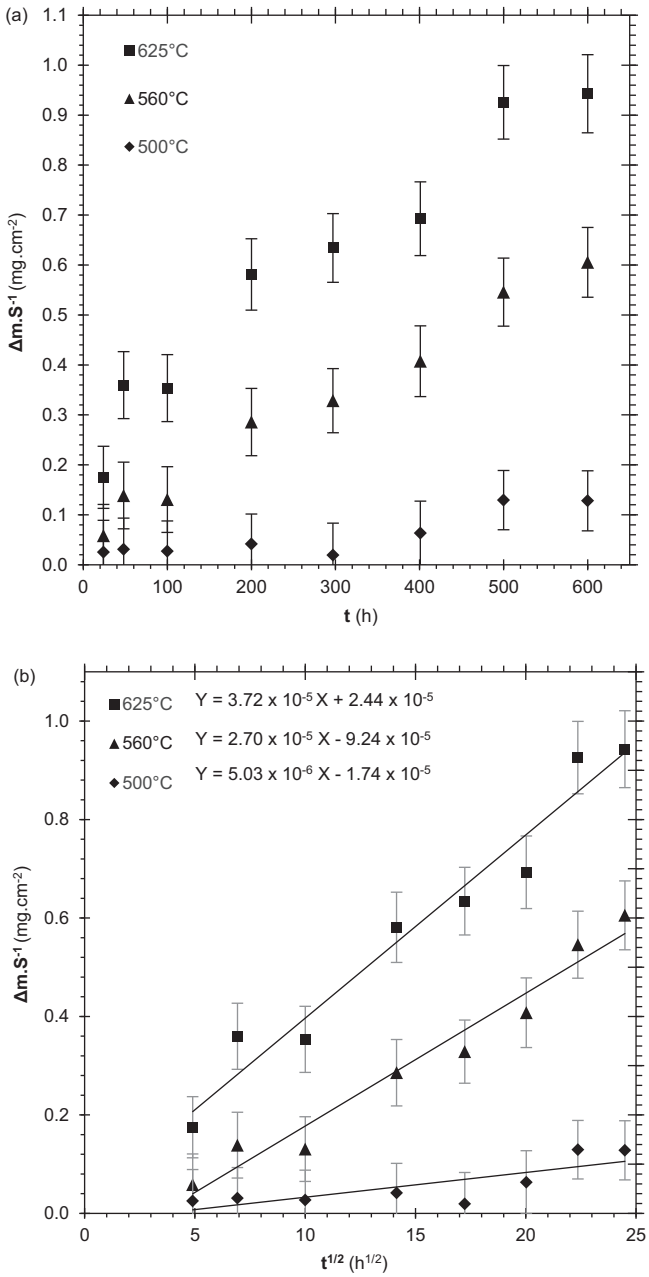

Fig. 1. Weight gain per unit area evolution with time of samples oxidized in laboratory air for 600 h at 500 °C, 560 °C and 625 °C (a), and weight gain per unit area evolution with time square root of same samples (b).

Table 1
Average chemical composition of the as received Ti-6Al-4V alloy, obtained by EDS analysis.

Elements	Al	Ti	V
Chemical composition (wt.%)	6	90	4
Chemical composition (at.%)	11	86	3

1.1. Material and methods

Ti-6Al-4V alloy used in this study is a Ti-based alloy, containing 6 wt.% Al and 4 wt.% V (Table 1). It has a biphase structure composed of α (HCP) phase and β (CC) phase. Rectangular samples

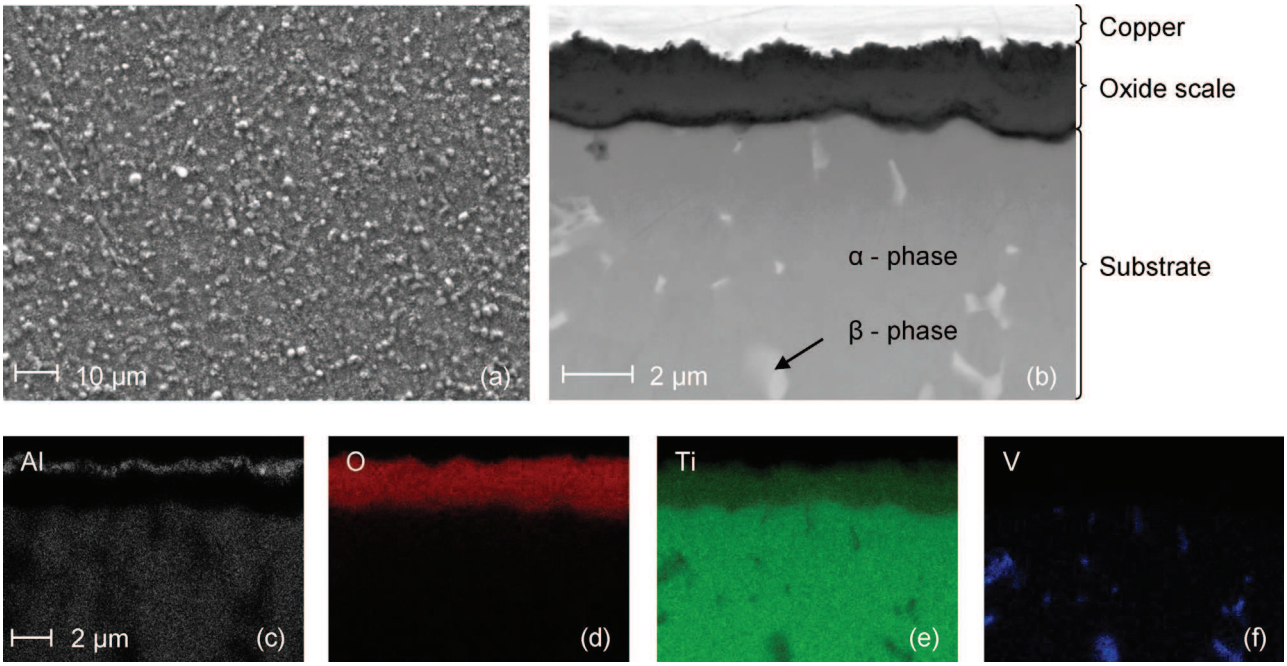

Fig. 2. SEM micrograph of a sample of Ti-6Al-4V oxidized in laboratory air at 560 °C for 600 h, (a) surface, (b) cross-section, and corresponding X-ray maps of Al (c), O (d), Ti (e) and V (f) elements.

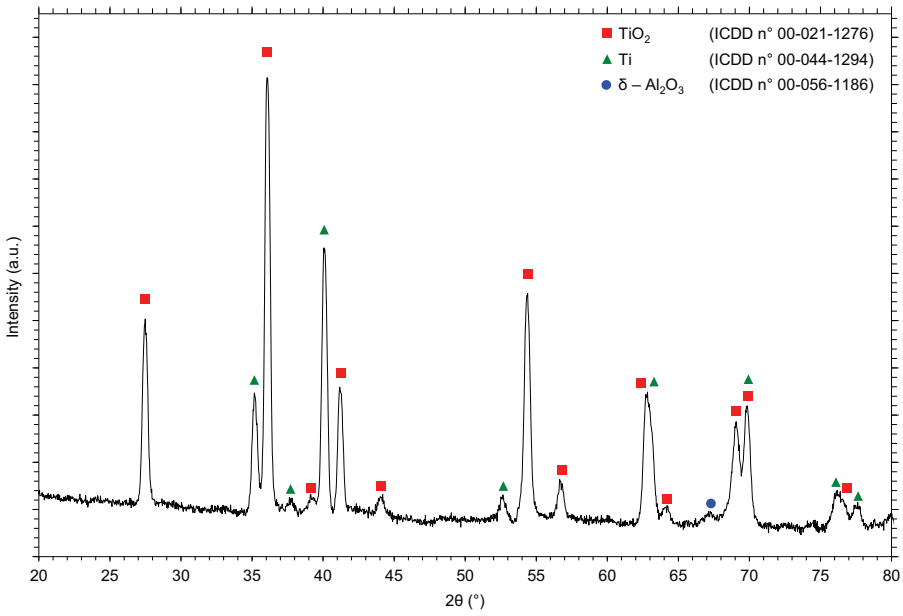

Fig. 3. Diffraction pattern of the XRD analysis performed on a sample of Ti-6Al-4V oxidized in laboratory air at 560 °C for 600 h.

measure approximately 16 mm x 9.0 mm and are 1.0 mm thick. All the specimens were mechanically grinded on SiC papers up to 600 grit [18–20,24], and were then cleaned in ethanol.

NaCl deposits were performed, by spraying in several steps, an aqueous saturated NaCl solution on the samples surfaces which were preheated at 60–80 °C. This method leads to a homogeneous and continuous deposit with a NaCl amount of 3–4 mg cm^{-2}.

Samples exposed at laboratory air, with and without NaCl deposit, were exposed to laboratory air in Carbolite CWF 1300 muffle furnaces. Air oxidation was performed at three temperatures (500 °C, 560 °C and 625 °C) for eight durations (24, 48, 100, 200, 300, 400, 500 and 600 h) to establish discontinuous weight gain measurements. Exposition to moist air (12 vol.% $H_2O_{(g)}$), with and without NaCl deposit, was done in an experimental tubular furnace at 560 °C during 600 h. Air enrichment in water vapour is performed by bubbling air in a round bottom flask of distilled water heated at 100 °C, which leads to water vapour saturated air. This mixture passes then through a condenser tube which is heated at 25 °C to set the quantity of water vapour at 12 vol.%, measured with an hygrometer [25]. The steam then passes through the furnace tube with a flow of 8 mL min^{-1}.

All samples were analysed in two successive steps. Surfaces were first characterized, followed by cross-sections analysis of the same samples. Preparation of cross-sections consisted of 4 steps. At first, a thin layer of Au was sputtered on each sample surface. Then, samples were coated with Cu by an electrolytic method. They were

finally coated in carbon doped phenolic resin and polished up to the mirror finishing.

The oxide surface and cross-section morphologies were analysed using a JEOL JSM-7600F scanning electron microscope. The chemical composition of the corrosion products was obtained by energy dispersive X-ray spectroscopy (EDS). Phase composition of the oxide scales was determined by X-ray diffraction with an Inel CPS 120 diffractometer using Cu Kα (λ = 0.154 nm) radiation with fixed incidence angle from 1° to 12° in function of corrosion scales thickness. The micro-hardness of each sample was evaluated with a BUEHLER 1600–6100 apparatus using a Vickers diamond head with a charge of 10 g, leading to indentation prints between 5 and 10 μm. Measurement points were done on the whole thickness of the metallic material, each 10 μm near the surface (for the first 100 μm), each 100 μm from 100 μm to 500 μm and then each 500 μm from 500 μm to the last 500 μm in the middle of the sample.

Thermodynamics calculations were performed with the Factsage 6.4™ software in order to propose corrosion mechanisms.

2. Results

2.1. Laboratory air oxidation

The evolution with time of the weight gains per unit area of the samples oxidized under laboratory air at 500 °C, 560 °C and 625 °C for 600 h are presented in Fig. 1a. The oxidation approximately follows a parabolic rate law at the three considered temperatures, according to Fig. 1b. The k_p values obtained from these linearized curves are 7.0×10^{-15} g^2 cm^{-4} s^{-2}, 2.0×10^{-13} g^2 cm^{-4} s^{-2} and 3.8×10^{-13} g^2 cm^{-4} s^{-2} respectively, according to the following formula:

$$\frac{\Delta m}{S} = \sqrt{k_p t} \quad (1)$$

where Δm is the weight gain per unit area in g cm^{-2}, S is the sample surface area in cm^2, t is the time in s and k_p is the parabolic constant of oxidation in g cm^{-2} s^{-1}. There are in the literature, only two available values of k_p for shorter durations of oxidation than 600 h. The first (1.7×10^{-12} g^2 cm^{-4} s^{-2}), proposed by Siab et al. [1], was determined after an oxidation treatment of 5.5 h at 600 °C. The second (3.0×10^{-12} g^2 cm^{-4} s^{-2}), was proposed by Zhang et al. [26] and determined from an oxidation treatment of 50 h at 600 °C. These values are both higher than the one determined in this study at 625 °C after 600 h oxidation. These differences could be explained by a transient effect, which is known to lead to faster kinetics at the beginning of the oxidation, as it can be noticed on the kinetic curve relative to 625 °C oxidation (Fig. 1a).

Surface observation of the sample treated during 600 h at 560 °C in laboratory air shows a homogeneous aspect composed of fine oxide grains (Fig. 2a). EDS analysis indicate the presence of Ti, O and Al (respectively 23 at.%, 68 at.% and 9 at.%). This result coupled with XRD analysis (Fig. 3) indicates mainly the presence of rutile TiO_2 (ICDD n° 00-021-1276), and δ-Al_2O_3 transient alumina (ICDD n° 00-056-1186).

Cross section samples (Fig. 2b) reveal the presence of a thin (2 μm), dense and adherent oxide layer. EDS elementary maps (Fig. 2c,d,e,f) reveal that aluminium oxide is at the outer part of the corrosion layer (≈ 300 nm), whereas titanium oxide is in the inner part (≈1.7 μm).

Inside the metallic substrate, light regions enriched in V can be observed, corresponding to the β-phase present in the Ti-6Al-4V alloy. The dark grains are Al-rich and correspond to the α-phase. Fig. 4 presents the micro-hardness profile versus the distance from the metal/oxide interface. The oxygen EDS profile is equally presented. A very large hardness value of $760HV_{0.01}$ is measured at the external part of the substrate close to the metal/oxide interface. Then the hardness value fastly decreases with the distance from the metal/oxide interface: at around 20 μm, it reaches the average value measured for the Ti-6Al-4V bulk alloy ($290HV_{0.01}$). In parallel, the O content equally decreases from 44 at.% at the interface to 5 at.% at 10 μm from the interface. It should be noted here that because of O surface pollution, the O content measured by EDS is certainly over-evaluated of several at.%. Therefore the above values should not be taken as quantitative. These evolutions prove the oxygen dissolution in the Ti-6Al-4V metallic substrate resulting in an important evolution of the mechanical properties. Fig. 4 allows evaluating the oxygen dissolution area thickness to around 10 μm.

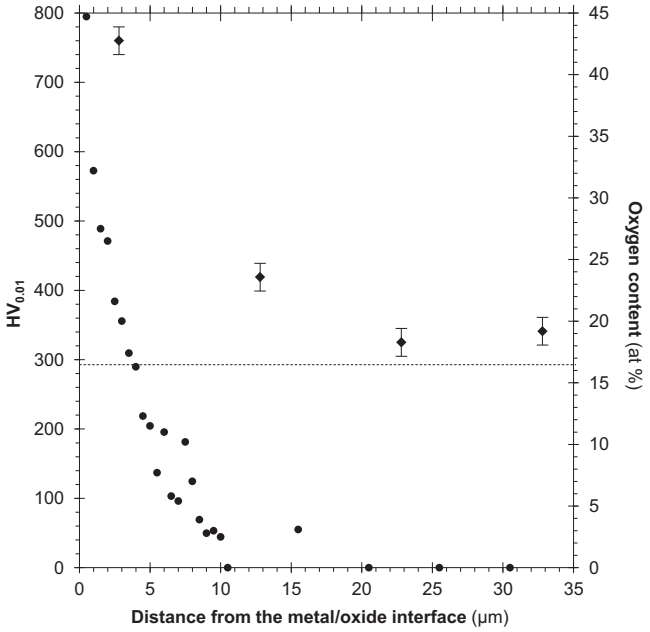

Fig. 4. Micro-hardness (♦) and relative oxygen content (●) (obtained by EDS) profiles versus distance from the metal/oxide interface Ti-6Al-4V oxidized in laboratory air at 560 °C for 600 h.

2.2. Moist air oxidation

The weight gain per unit area is slightly lower after 600 h exposure at 560 °C in moist air (0.415 ± 0.065 mg cm^{-2}) than under laboratory air in the same conditions (0.605 ± 0.07 mg cm^{-2}).

The surface morphology of the sample exposed to wet air is very similar to that observed after the laboratory air treatment (Fig. 5a). The oxide layer is homogeneous and composed of fine grains. EDS analysis performed on this surface indicate the presence of Ti, O and Al (respectively 24 at.%, 66 at.% and 10 at.%). Cross-section observations reveal that the scale is thin (2 μm), dense and adherent to the metallic substrate (Fig. 5b). The previous EDS analysis coupled with EDS elementary mapping (Fig. 5c–f) and XRD (Fig. 6) indicates that the oxide scale is composed of an outer alumina layer (≈600 nm) (ICDD n° 01-080-0955) and an inner rutile layer (≈1.4 μm) thick (ICDD n° 00-021-1276).

Fig. 7 presents the micro-hardness profile and the O content as a function of the distance from the metal/oxide interface. Results are similar to those observed for the oxidation in laboratory air. The same value of hardness of $760HV_{0.01}$ is measured at the external part of the substrate. This hardness value fastly decreases with the distance from the metal/oxide interface: at 20 μm, it is stabilised to a value close to the average value measured for raw Ti-6Al-4V. In parallel, the O content also decreases from 28 at.% to 3 at.% at 10 μm from the interface. In consequence, the oxygen dissolution area thickness can be evaluated to around 10 μm. Here again,

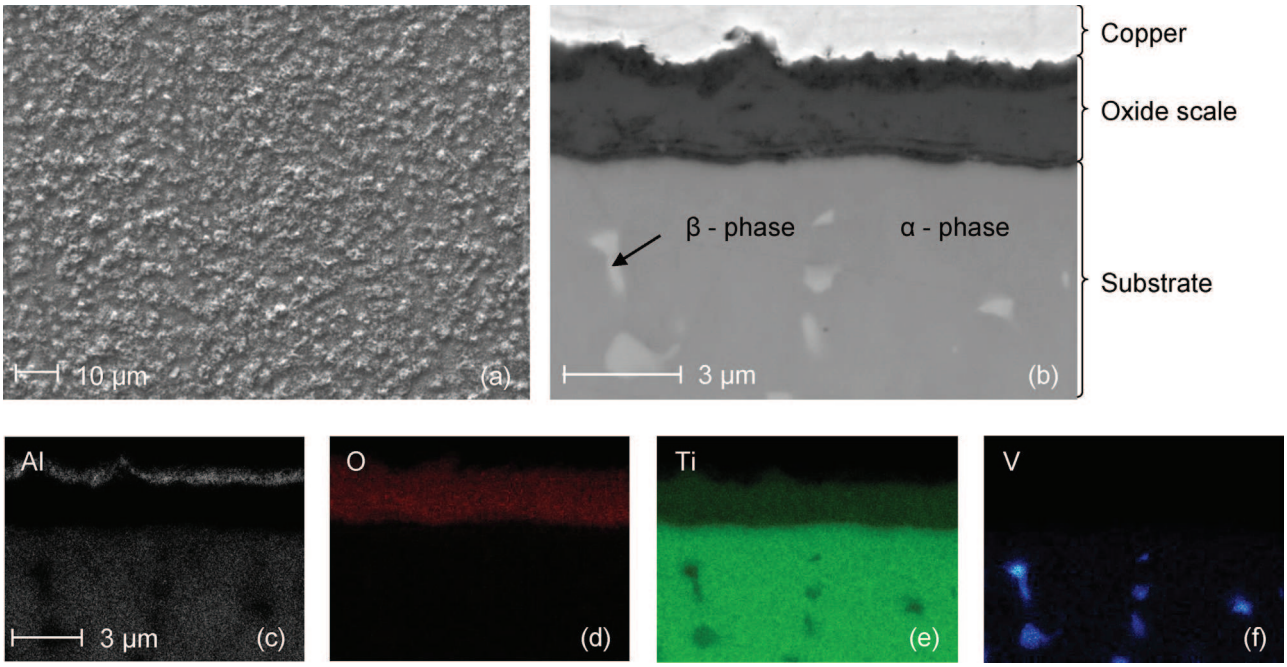

Fig. 5. SEM micrograph of a sample of Ti-6Al-4V oxidized in moist air at 560 °C for 600 h, (a) surface, (b) cross-section, and corresponding X-ray maps of Al (c), O (d), Ti (e) and V (f) elements.

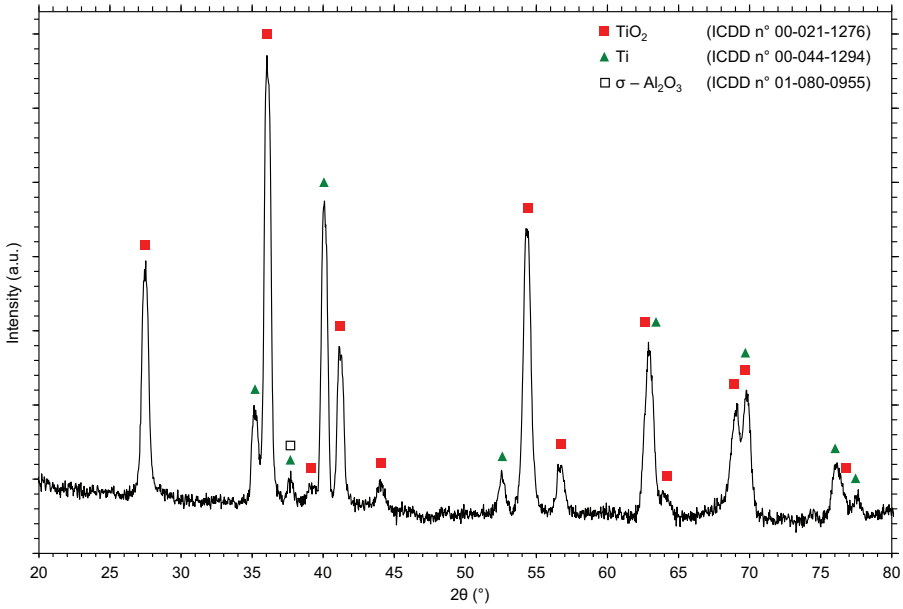

Fig. 6. Diffraction pattern of the XRD analysis performed on a sample of Ti-6Al-4V oxidized in moist air at 560 °C for 600 h.

as explained before, the O content measured by EDS suffers from surface pollution and is certainly over evaluated of several at.%.

2.3. NaCl induced corrosion in air

NaCl coated sample exposed for 600 h at 560 °C to laboratory air show a weight gain per unit area 5 times higher than the sample exposed to laboratory air in the same conditions (Fig. 8).

Surface observations of the sample (Fig. 9) reveal a heterogeneous aspect with blisters and cracked corrosion products. EDS analysis indicate the presence of Ti, O and Na (respectively 22 at.%, 64 at.% and 14 at.%). Based on this average chemical composition, XRD analysis (Fig. 10) evidence the presence of rutile, TiO_2 (ICDD n° 01-070-7347), as the main phase and two types of sodium-titanium mixed oxides, $Na_4Ti_5O_{12}$ (ICDD n° 00-052-1814) and Na_xTiO_2 (ICDD n° 00-022-1404). In addition, XRD analyses performed at different times of oxidation (24, 48, 100, 200, 300, 400, 500 and 600 h) reveal an evolution of the mixed Na-Ti oxide phases ratio, the Na_xTiO_2 phase becoming preponderant at long times of oxidation.

Cross sections indicate the presence of a thick (35 µm), porous and non-adherent oxide layer on the material surface. This morphology is in agreement with the work of Dumas and St. John [18] on the NaCl coated IMI 685 alloy oxidized at 600 °C during 24 h. Presence of large cracks between metallic substrate and oxide layer can also be noticed (Fig. 11a). EDS elementary X-ray maps (Fig. 11b–h)

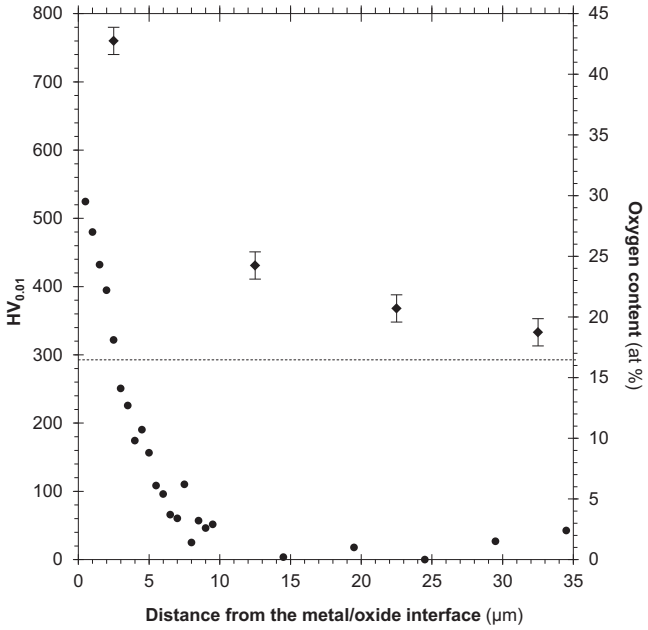

Fig. 7. Micro-hardness (♦) and relative oxygen content (●) (obtained by EDS) profiles versus distance from the metal/oxide interface Ti-6Al-4V oxidized in moist air at 560 °C for 600 h.

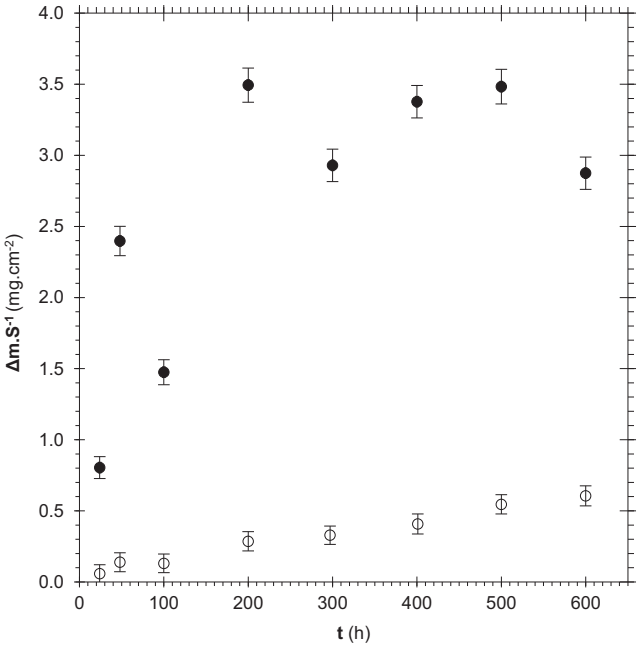

Fig. 8. Weight gain per unit area evolution with time of samples oxidized in laboratory air with (●) and without (○) NaCl deposit for 600 h at 560 °C.

show that the oxide scale is formed of four different layers. The outer part is a mixed sodium-titanium oxide which, in agreement to XRD surface and EDS analyses, should correspond to Na_xTiO_2 type (with x close to 0.23, according to the XRD pattern) and $Na_4Ti_5O_{12}$ phases. Just below this layer, there is a very thin aluminium rich oxide, which was not detected by XRD, certainly because of its small amount. The two inner layers are titanium oxides with different Ti contents (the Ti content seems to be higher in the closest part to the metal/oxide interface). Taking into account the XRD results, the outer part of this titanium oxide layer should correspond to TiO_2. However, it is very difficult to identify whether the inner part corresponds to a different phase, as its position with respect to the

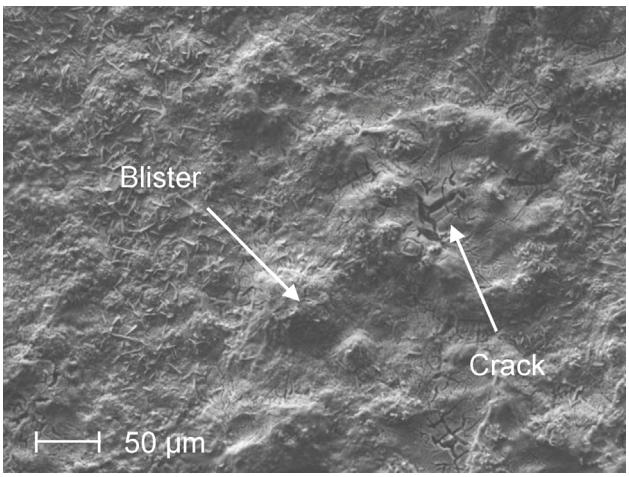

Fig. 9. SEM surface micrograph of Ti-6Al-4V oxidized in laboratory air with a NaCl deposit at 560 °C for 600 h.

sample surface makes it difficult to be reached by the X-rays. However, according to EDS quantitative analysis (41 at.% of Ti, 51 at.% of O, 5 at.% of Al, and 3 at.% of V), this phase should correspond to TiO with a small proportion of addition elements. Presence of a small amount of Cl can also be noticed in this Ti layer that is the closest to the metal/oxide interface. This interface is the less adherent and location for initiation of corrosion product spallation. The outer part of the metallic substrate presents an Al rich layer that was not observed during the previous tests without NaCl deposit.

Fig. 12 presents the micro-hardness profile and the O content versus the distance from the metal/oxide interface. The oxygen content is constant and close to 0 at.%, showing the absence of any oxygen dissolution area. Even if the micro-hardness profile stays constant on the whole thickness of the sample, it nevertheless shows a small decrease at each side of the metallic substrate, corresponding to the first 5 µm from the metal/oxide interface, probably related to the effect of approach of the porous area.

2.4. NaCl induced corrosion in moist air

The sample exposed 600 h at 560 °C to moist air with a NaCl deposit shows a weight gain per unit area 15 times higher than the uncoated samples exposed in laboratory and moist air.

Surface observations (Fig. 13) of the sample indicate a heterogeneous aspect with large cavities. EDS analysis indicates the presence of Ti, O and Na (respectively 25 at.%, 65 at.% and 10 at.%). This indicative chemical composition coupled with XRD (Fig. 14) analysis indicates the presence of several kinds of titanium oxide: rutile TiO_2 (ICDD n° 01-070-7347) as the main phase, but also Ti_2O_3 (ICDD n° 00-043-1033) and TiO (ICDD n° 00-012-0754). Two types of sodium-titanium mixed oxides, $Na_4Ti_5O_{12}$ (ICDD n° 00-052-1814) and Na_2TiO_3 (ICDD n° 00-037-0345), are also identified.

Cross section observations (Fig. 15a) evidence the presence of a very thick (90 µm), porous and non-adherent oxide layer on the material surface. The presence of a large crack inside the corrosion products layer can also be observed. EDS elementary X-ray maps (Fig. 15b–h) reveal that the oxide layer is stratified into four parts. The outer part is thin (≈ 5 µm) and porous and corresponds to mixed sodium-titanium oxide, which is probably a mixture of $Na_4Ti_5O_{12}$ and Na_2TiO_3 according to XRD results. The three layers below are titanium oxide with an increasing Ti content. EDS quantifications done in several regions of these different layers suggest that they correspond to TiO_2 (32 at.% for Ti and 68 at.% for O), Ti_2O_3 (41 at.% for Ti and 59 at.% for O) and TiO (48 at.% for Ti and 52 at.% for O), respectively. A small amount of Cl is present inside the

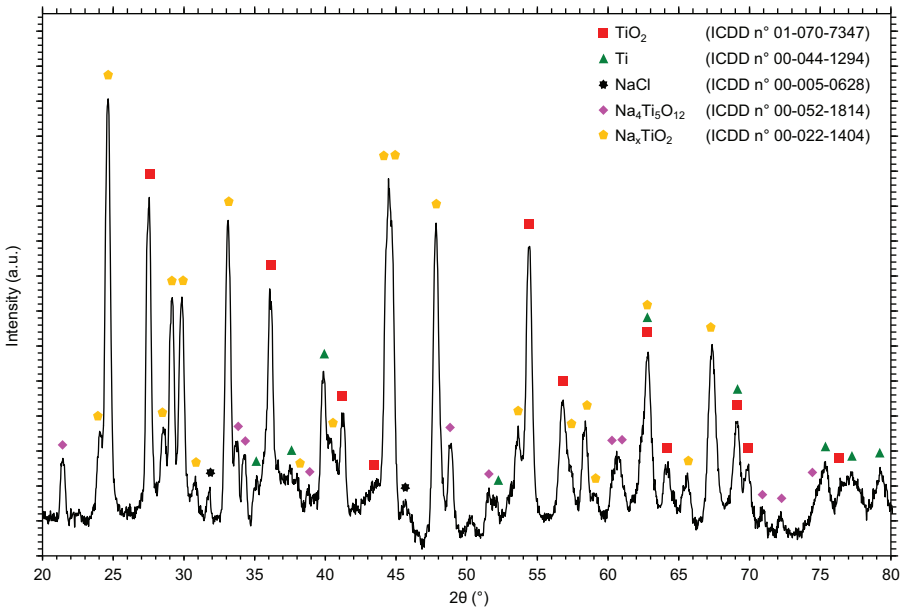

Fig. 10. Diffraction pattern of the XRD analysis performed on a sample of Ti-6Al-4V oxidized in laboratory air with a NaCl deposit at 560 °C for 600 h.

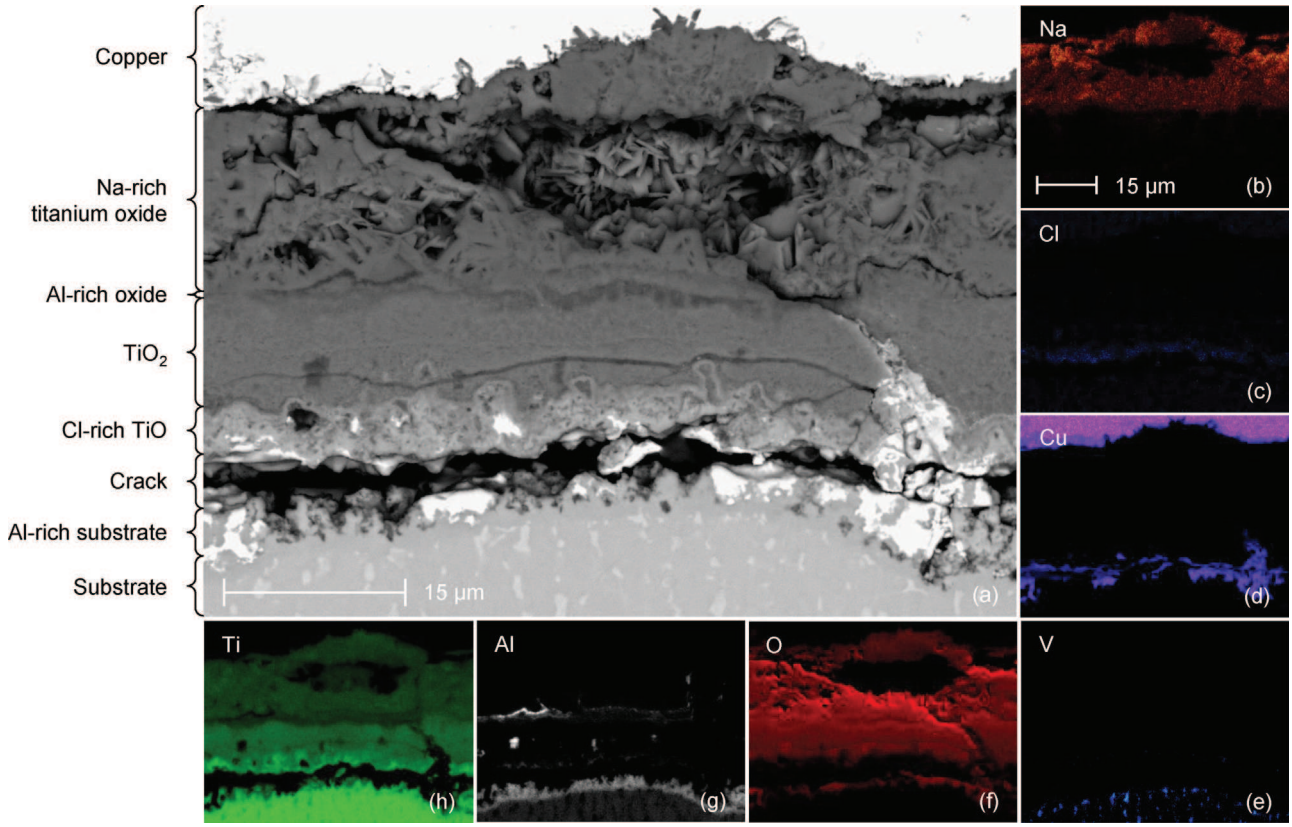

Fig. 11. SEM micrograph of a sample of Ti-6Al-4V oxidized in laboratory air with a NaCl deposit at 560 °C for 600 h, (a) cross-section and corresponding X-ray maps of Na (b), Cl (c), Cu (d), V (e), O (f), Al (g) and Ti (h) elements.

inner titanium oxide layer near the interface with the metal. The oxide layer adherence at this interface is very poor and can lead to spallation. As in the case of the NaCl coated sample exposed to air, at the external part of the metallic substrate, an Al-rich layer was observed, corresponding to a Ti depletion.

Fig. 16 presents the micro-hardness profile and the O content as a function of the distance from the metal/oxide interface. Unlike the results of Gurrappa [21], the absence of variation in oxygen profile and mainly the 0 at.% value, demonstrate the absence of an oxygen dissolution area. Even if the micro-hardness profile stays constant all across the sample, it nevertheless shows a low decrease at each ends of the metallic substrate, corresponding to the first 20 µm from the metal/oxide interface.

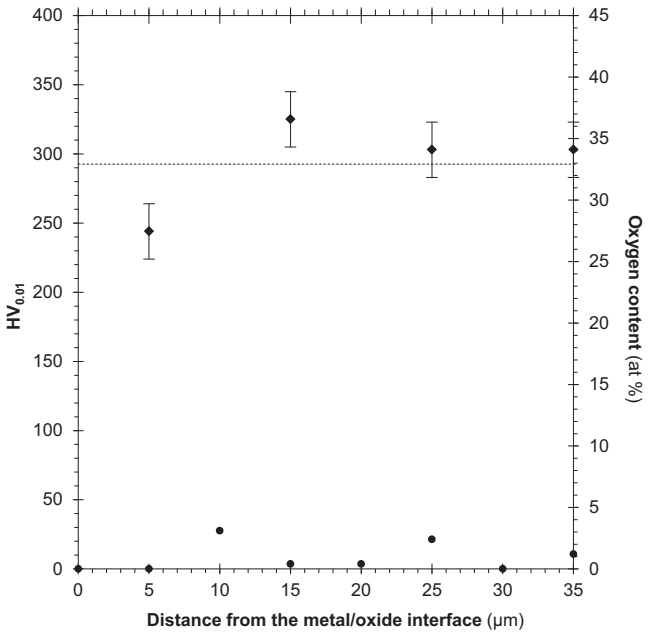

Fig. 12. Micro-hardness (♦) and relative oxygen content (●) (obtained by EDS) profiles versus distance from the metal/oxide interface Ti-6Al-4V oxidized in laboratory air with a NaCl deposit at 560 °C for 600 h.

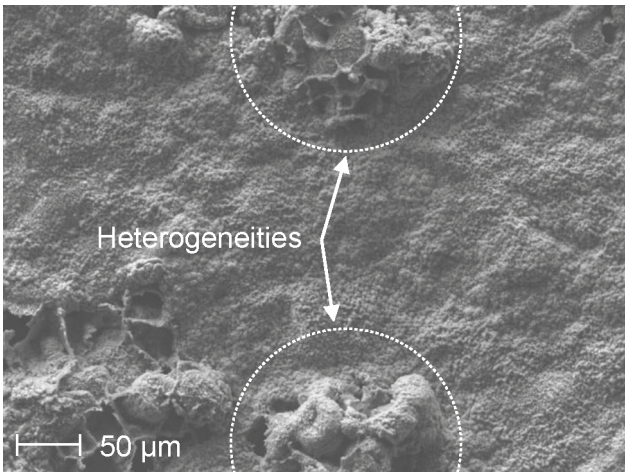

Fig. 13. SEM surface micrograph of Ti-6Al-4V oxidized in moist air with a NaCl deposit at 560 °C for 600 h.

3. Discussion

In laboratory air, Ti-6Al-4V oxidation followed a parabolic rate law. Corrosion products were stratified with alumina in the outer part and rutile in the inner part of the oxide scale, after oxidation at 560 °C for 600 h. These observations are in accordance with previous papers [1–4]. Titanium alloys are known to allow dissolution of oxygen in the substrate below the oxide scale [3,5,6], leading to a decrease of ductility. This oxygen dissolution area reached around 10 μm depth; it is in agreement with previous results of Guleryuz et al. [3,5].

The Ti-6Al-4V alloy presented the same behaviour in moist air as in laboratory air at 560 °C after 600 h exposure. Similar thickness, oxide phases and stratification of the oxide scale can be observed on both samples. These results are partially in agreement with previous studies on the water vapour effect on Ti alloys oxidation. For example, Motte et al. [7] observed on Ti-6Al-4V, an intermediate alumina enrichment inside the rutile scale in different conditions

Table 2
Standard free enthalpy formation and equilibrium constants of reaction $NaCl_{(s)} \leftrightarrow NaCl_{(g)}$ (determined by FactSage 6.4/Fact PS – FTSalt – thermodynamic calculation using reaction module for 1 mol of species).

T (K)	T (°C)	ΔG° (kJ mol^{-1})	K_{eq}
733	460	+117.84	4.01×10^{-9}
783	510	+110.76	4.09×10^{-8}
833	560	+103.74	3.12×10^{-7}
883	610	+96.79	1.88×10^{-6}

of temperature (850 °C) and humidity ($P(H_2O) \approx 220$ Pa). In parallel, Pérez et al. [9] showed that in the same temperature range (700 °C), the oxide layers are equivalent after exposures of pure Ti in dry and moist air, but using a dewpoint of 8 °C which corresponds to a very low concentration in water (≈ 1 vol.%). The same oxidation kinetics are equally observed. However, the oxygen diffusion thickness is slightly higher under moist air than in dry air. These observations were related to different oxidant species in moist air. The adsorption of water molecules on the rutile surface leads to their dissociation in H^+ and OH^- ions [27]. Due to its smaller size compared to O^{2-}, OH^- is supposed to diffuse more rapidly [10], resulting in faster oxidation kinetics (including the formation of the oxide scale and the formation of the oxygen dissolution area) with increasing the water vapour pressure. The differences between the results of the present study and those of the literature could be due to the temperature, which is lower in the present study. It could also be due to the alloying elements, which are known to influence the behaviour of the materials under oxidative conditions. Zeller et al. [27] previously showed that increasing the Al-content of the Ti alloys reduced the difference between the water vapour containing atmosphere and dry air. For Ti-Al alloys able to form protective alumina scales, no significant effect of the water vapour on the oxidation kinetics was reported [27]. The influence of water vapour strongly depends on the volume contents of TiO_2 and Al_2O_3 in the oxide scale.

The NaCl deposit was shown to be extremely harmful for the material behaviour in laboratory air; the weight gain per unit area being 5 times higher than for the NaCl free sample, while the oxide thickness was more than 15 times higher. This increase and slightly different evolution of weight gains (despite the presence of some divergent values) (Fig. 8) suppose the existence of a different oxidation mechanism. Moreover, presence of pores, blisters, cracks and the poor adherence of the oxide scale to the substrate are complementary evidences of the detrimental behaviour of Ti-6Al-4V in active corrosion conditions. The few studies previously done on the NaCl induced oxidation of the Ti alloys did not allow to clearly identify the reaction mechanism, mainly because of the lack of thermodynamic data needed to confirm the formation of such complex corrosion layers. Xiong et al. [24] suggested, in the case of the Ti60 alloy, that pores and cracks could be due to the rapid inward diffusion of corrosive species through the channels (porosity and cracks) in the corrosion products up to the metal/oxide interface. This accelerated corrosion was explained by the authors through the reaction of titanium dioxide with NaCl to form a mixed titanium-sodium oxide and a volatile chloride [23,24,28], supported by some thermodynamic calculations. However, the mechanism could not be completely demonstrated because of the lack of some thermodynamic data and positive value of standard free enthalpy for the initiating reaction.

Knowing that $NaCl_{(s)}$ melts at 800 °C and vaporizes at 1515 °C [29,30], it is obvious that NaCl remains essentially solid at the corrosion test temperature 560 °C (positive ΔG° for the sublimation of $NaCl_{(s)}$ (Table 2)).

In previous studies related to active oxidation beneath molten salts deposit, it has been demonstrated that if there is no pre-existent chlorine in the gas phase, the chlorine source must be

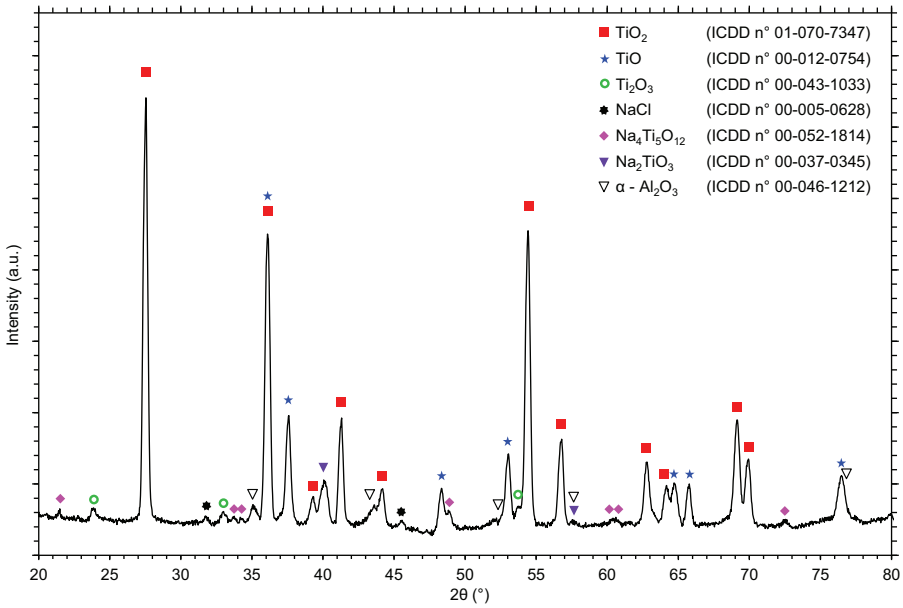

Fig. 14. Diffraction pattern of the XRD analysis performed on a sample of Ti-6Al-4V oxidized in moist air with a NaCl deposit at 560 °C for 600 h.

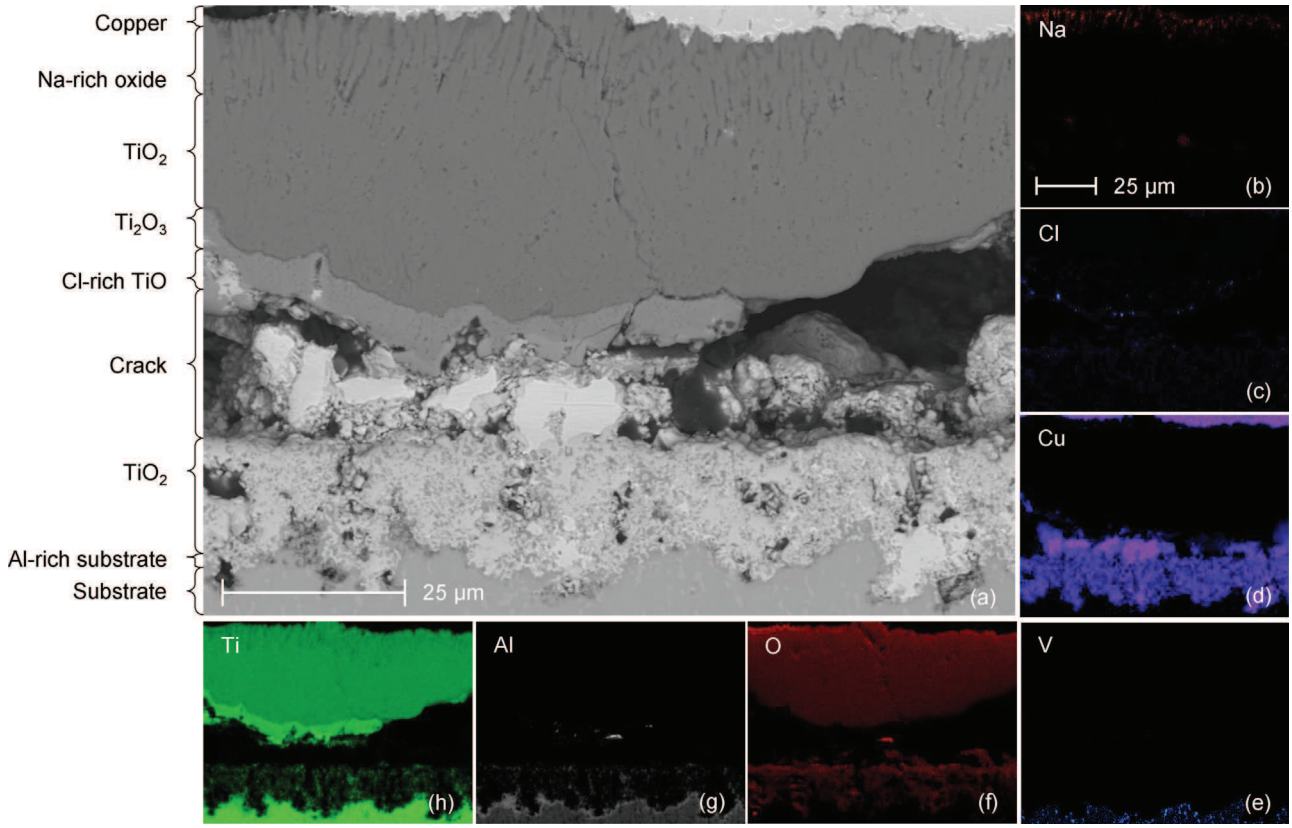

Fig. 15. SEM micrograph of a sample of Ti-6Al-4V oxidized in moist air with a NaCl deposit at 560 °C for 600 h, (a) cross-section and corresponding X-ray maps of Na (b), Cl (c), Cu (d), V (e), O (f), Al (g) and Ti (h) elements.

the molten chlorides [31,32]. In these studies case, chlorine can be released by the oxidation of the molten chloride. However, in our case the sodium chloride is not melted and cannot be oxidized at the given test temperature according to predominance diagram Fig. 19. Thus another source of chlorine should exist and the following hypothesis is suggested.

It is well known that for any liquid compound, equilibrium between liquid and gaseous states is established, leading to the creation of a vapour pressure of this compound (mainly dependent of the temperature). This phenomenon, at a lesser extent, is also true for solids [33,34]. Considering constant equilibrium between $NaCl_{(s)}$ and $NaCl_{(g)}$ (Eq. (2)), it appears that NaCl vapour pressure at 560 °C is around 3.12 10^{-7} bar, according to Table 2, Fig. 17 and

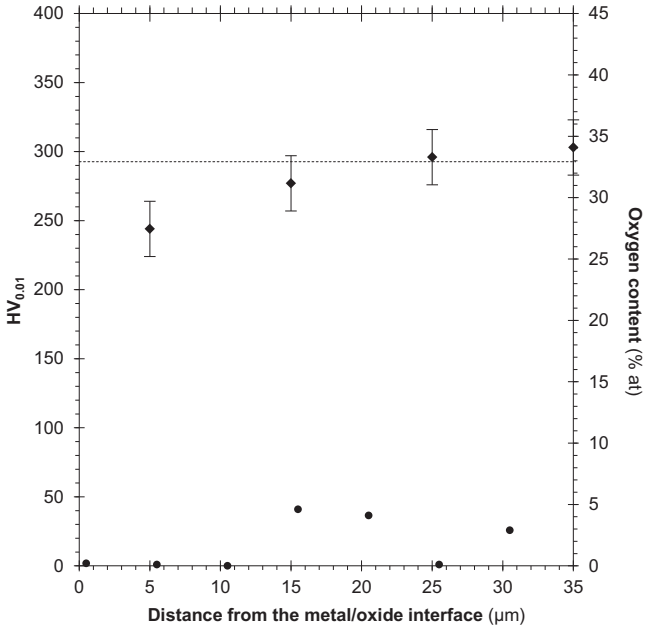

Fig. 16. Micro-hardness (♦) and relative oxygen content (●) (obtained by EDS) profiles versus distance from the metal/oxide interface Ti-6Al-4V oxidized in moist air with a NaCl deposit at 560 °C for 600 h.

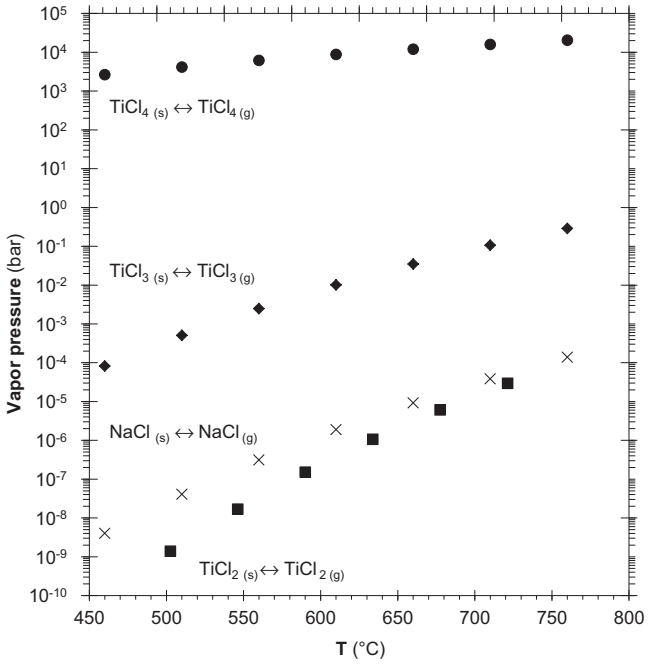

Fig. 17. Vapor pressure evolutions of major chloride compounds formed by the reaction of NaCl with Ti-6Al-4V in air, and vapour pressure of NaCl between 460 °C and 760 °C (determined by FactSage 6.4/Fact PS – FTSalt – thermodynamic calculation using reaction module for 1 mol of species).

literature [35,36]. Thus, this vapour pressure cannot be neglected. The equilibrium constant given in Table 2 is calculated as:

$$K = \frac{a_{NaCl_{(g)}}}{a_{NaCl_{(s)}}} \quad (2)$$

with $a_{NaCl_{(s)}} = 1$. There are experimentally two evidences that this equilibrium occurs. The first is the observation of the morphology of NaCl grains after oxidation. Instead of presenting sharp edges of as crystallised grains, NaCl grains present rounded edges (Fig. 18),

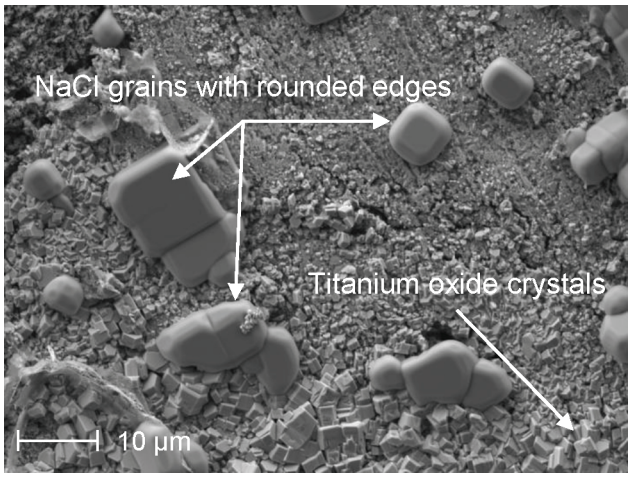

Fig. 18. SEM surface micrograph of the metal|oxide interface of Ti-6Al-4V oxidized in laboratory air with a NaCl deposit at 560 °C for 600 h, presenting some NaCl grains with rounded edges.

Table 3
Reactions proposed for the mechanisms of active corrosion and their corresponding calculated values of standard free enthalpy (calculated with FactSage 6.4 using reaction module and FactPS/FT Oxid and FTSalt database).

No.	Equilibrium equation	ΔG°_{833K} (kJ mol^{-1})
(3)	$4NaCl_{(s)} + O_{2(g)} + 2TiO_{2(s)} \leftrightarrow 2Na_2TiO_{3(s)} + 2Cl_{2(g)}$	+ 281.04
(4)	$4NaCl_{(g)} + O_{2(g)} + 2TiO_{2(s)} \leftrightarrow 2Na_2TiO_{3(s)} + 2Cl_{2(g)}$	−133.57
(5)	$4NaCl_{(g)} + O_{2(g)} + 5TiO_{2(s)} \leftrightarrow Na_4Ti_5O_{12(s)} + 2Cl_{2(g)}$	/
(6)	$Ti_{(s)} + 2Cl_{2(g)} \leftrightarrow TiCl_{4(g)}$	−662.54
(7)	$TiCl_{4(g)} + O_{2(g)} \leftrightarrow TiO_{2(s)} + 2Cl_{2(g)}$	−129.94
(8)	$4NaCl_{(s)} + 2H_2O_{(g)} + TiO_{2(s)} \leftrightarrow 2Na_2TiO_{3(s)} + 4HCl_{(g)}$	+143.91
(9)	$4NaCl_{(g)} + 2H_2O_{(g)} + TiO_{2(s)} \leftrightarrow 2Na_2TiO_{3(s)} + 4HCl_{(g)}$	−64.06
(10)	$4NaCl_{(g)} + 2H_2O_{(g)} + 5TiO_{2(s)} \leftrightarrow Na_4Ti_5O_{12(s)} + 4HCl_{(g)}$	/
(11)	$Ti_{(s)} + 4HCl_{(g)} \leftrightarrow TiCl_{4(g)} + 2H_{2(g)}$	−263.89
(12)	$2H_2O_{(g)} + 2Cl_{2(g)} \leftrightarrow 4HCl_{(g)} + O_{2(g)}$	+4.68

which may attest of their progressive gas releasing (to maintain the solid ↔ gas equilibrium at the given temperature). Secondly, this phenomenon has also been verified by exposing an uncoated sample to gaseous environment including a crucible containing $NaCl_{(s)}$ upstream. The characterisations of this sample revealed the presence of Na on the sample surface, which suppose a transport of the NaCl through the gas flow to the sample surface, accrediting the thesis of a gaseous state for NaCl.

Moreover, calculations of standard free enthalpies provide positive values for reactions involving solid NaCl (Eq. (3) in Table 3), whereas negative values are obtained with gaseous NaCl (Eq. (4)).

$$4NaCl_{(s)} + O_{2(g)} + 2TiO_{2(s)} \leftrightarrow 2Na_2TiO_{3(s)} + 2Cl_{2(g)} \quad (3)$$

$$4NaCl_{(g)} + O_{2(g)} + 2TiO_{2(s)} \leftrightarrow 2Na_2TiO_{3(s)} + 2Cl_{2(g)} \quad (4)$$

In consequence, initiating reaction between NaCl, O_2 and TiO_2 should involve gaseous NaCl instead of solid NaCl. According to thermodynamic predictions, these considerations are valid for reaction involving Na-Ti oxides, which are referenced in databases as $(Na_2O)(TiO_2)_3$ (equivalent to $Na_2Ti_3O_7$), $(Na_2O)(TiO_2)_6$ (equivalent to $Na_2Ti_6O_{13}$) and Na_2TiO_3. But, SEM-EDS and XRD analyses

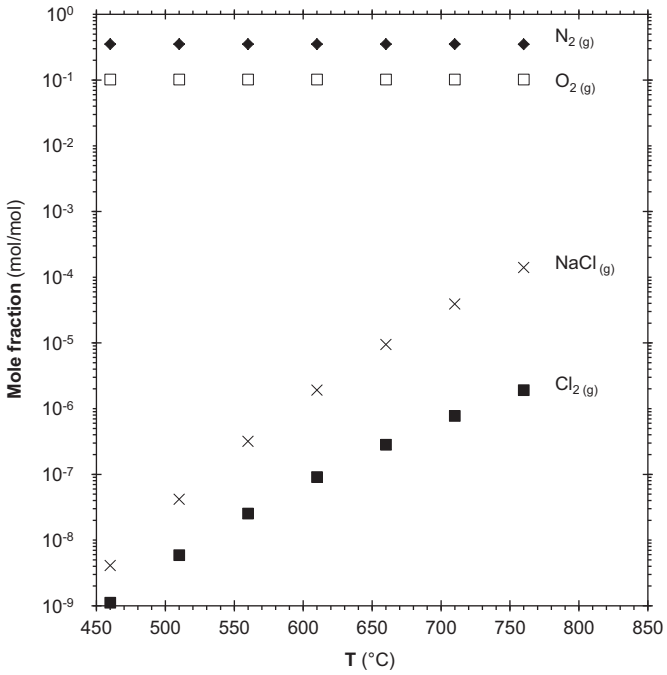

Fig. 19. Evolution of mole fractions of the major gaseous compounds present after the reaction between $TiO_{2(s)}$, $N_{2(g)}$, $O_{2(g)}$ and $NaCl_{(s)}$ in air, from 460 °C to 760 °C (determined by FactSage 6.4/ELEM – FactPS – FTSalt database/thermodynamic calculation using equilibrium module considering 1 g of each species).

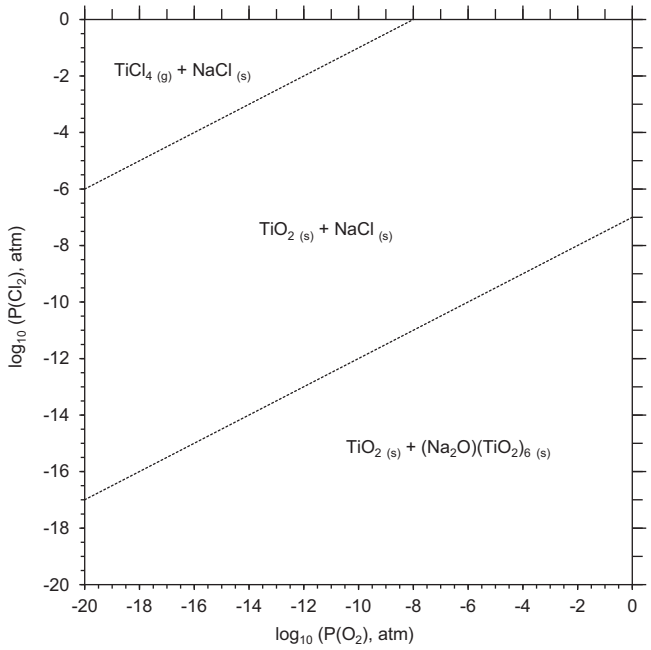

Fig. 20. Predominance diagram for species at 833 K for the sysytem Ti-Cl-O—Na established for 1 atm pressure using FactSage 6.4 from thermodynamic database FactPS/Elem/FT Oxyd.

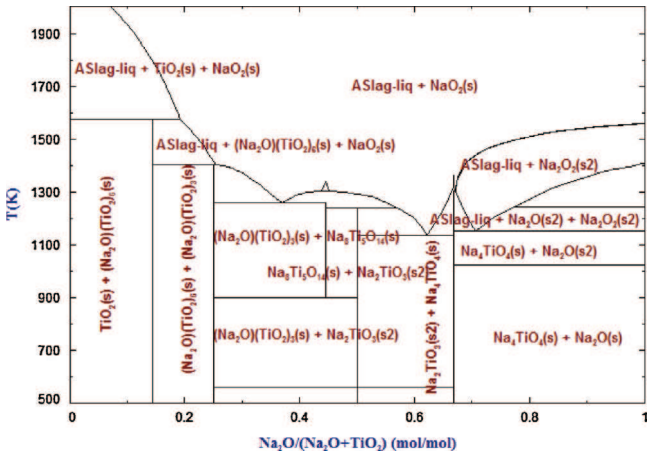

Fig. 21. TiO_2—Na_2O Binary Diagram established for 1 atm pressure using FactSage 6.4 from thermodynamic database FactPS/Elem/FT Oxyd.

evidenced the presence of $Na_4Ti_5O_{12}$ and Na_xTiO_2 (Eq. (5)) for which no thermodynamic data are available.

$$4NaCl_{(g)} + O_{2(g)} + 5TiO_{2(s)} \leftrightarrow Na_4Ti_5O_{12(s)} + 2Cl_{2(g)} \quad (5)$$

The assumption of the formation of $Cl_{2(g)}$ is confirmed by thermodynamic predictions of gaseous compounds present after the reaction 4 (Table 3, Fig. 19). In the experimental conditions of the present study, $Cl_{2(g)}$ appears to be the first of the major gaseous species that are formed during the reaction mentioned above. Moreover, according to the predominance diagram of species (Fig. 20), at 560 °C in high $P(O_2)$ and low $P(Cl_2)$ area (which would correspond to the oxide/atmosphere interface in the present case), NaCl should be destabilised, leading to the formation of a Na-Ti oxide in presence of TiO_2. This Na-Ti oxide would be $(Na_2O)(TiO_2)_6$, which would correspond to $Na_2Ti_6O_{13}$. As a consequence, the presence of both $Na_4Ti_5O_{12}$ and Na_xTiO_2 intermediate compounds (Fig. 21) suggests that the system would not be in the equilibrium state, which could lead to the formation of such compounds. The evolution of the $Na_4Ti_5O_{12}/Na_xTiO_2$ ratio with time, according to XRD analyses, could be another evidence of this non-equilibrium state.

However, it is rather difficult to state where this reaction takes place. In the present case, a majority of NaCl remains at the top of the oxide layer, while a few grains are presents inside the oxide scale and at the oxide/substrate interface, probably stabilised by the low $P(O_2)$ and the high $P(Cl_2)$, according to the predominance diagram of species (Fig. 20). This presence of NaCl grains at the top of the oxide layer supposes that the reaction of Eq. (4) would take place at the NaCl/native TiO_2 interface.

According to the hypothesis that $NaCl_{(g)}$ acts as precursor in the $Cl_{2(g)}$ releasing mechanism (Eq. (4)), it is supposed that only $Cl_{2(g)}$ takes part in the next mechanism steps. Thus, the as-released $Cl_{2(g)}$ can be then partially released in the atmosphere, but some might migrate down to the metal/oxide interface, according to its activity gradient, and react with metallic Ti in order to form a Ti chloride following the here below reaction (Eq. (6) in Table 3) with a high negative value of standard free enthalpy.

$$Ti_{(s)} + 2Cl_{2(g)} \leftrightarrow TiCl_{4(g)} \quad (6)$$

This reaction of $Cl_{2(g)}$ with $Ti_{(s)}$ at the metal/oxide interface will lead to a continuous evaporation of $TiCl_{4(g)}$, supporting an increased corrosion kinetics. The existence of this mechanism is experimentally supported by the residual presence of Cl in the part of the oxide layer closest to the metal/oxide interface (probably resulting from titanium chloride condensation during cooling and partially dissolved by water used for grinding). The rapid Ti consumption is proven by an Al enrichment at the metallic substrate surface and by the presence of a porous metal area below the substrate surface, in agreement with Xiong et al. results [24]. In parallel, the low adherence of corrosion products to the substrate also supports an active oxidation mechanism involving metallic chloride volatilisation.

According to the diagram of species predominance established as a function of O_2 and Cl_2 partial pressure (Fig. 20), $TiCl_{4(g)}$ is con-

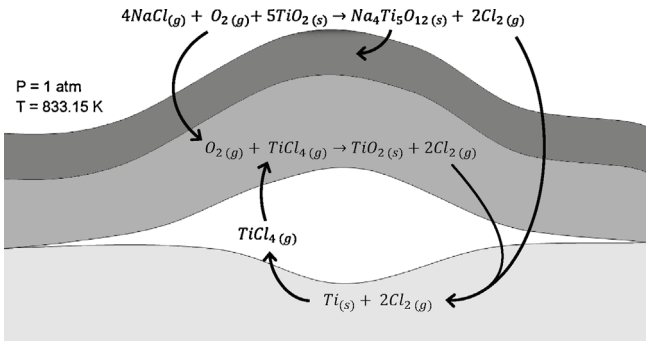

Fig. 22. Diagram of the high temperature cyclic corrosion mechanism of Ti-alloy by NaCl in air.

sidered to be the major compound formed by the reaction between Ti $_{(s)}$ and $Cl_{2(g)}$ (Eq. (6)) due to its stabilisation under high partial pressure of Cl_2 and low partial pressure of O_2, which is consistent with the expected atmosphere at the metal/oxide interface. Moreover, this titanium tetra-chloride appears to have the highest pressure vapour (Fig. 17) and in consequence, to be the most stable species of titanium chlorines in these experimental conditions.

The last step of the mechanism would involve the reaction of $TiCl_{4(g)}$ with the inward diffusing oxygen leading to the formation of titanium dioxide and gaseous chlorine (Eq. (7)):

$$TiCl_{4(g)} + O_{2(g)} \leftrightarrow TiO_{2(s)} + 2Cl_{2(g)} \quad (7)$$

In this way, gaseous Cl_2 is produced again and can be used to react with Ti as in reaction 4. The last two reactions will take place cyclically and keep the mechanism of active oxidation up.

Same reactional sequences could be applied to Al and V (with the formation of $AlCl_{3(g)}$ [24] and $VCl_{4(g)}$), however neither aluminium-sodium oxide nor vanadium-sodium oxide were put in evidence in our case. These reactions were probably not favoured thermodynamically and/or their kinetic was not dominant.

The three suggested steps of the mechanism of Ti corrosion in presence of NaCl (Eqs. (4), (6) and (7)) are summarised in Fig. 22.

Concerning the absence of an oxygen diffusion area, this finding also attests of the preponderance of the corrosion kinetics over the inward oxygen diffusion kinetics into the metal. The metal surface recession due to active corrosion is faster than the inward diffusion of oxygen, and then no O-enriched metal layer is found.

The detrimental effect of the NaCl deposit is increased in presence of water vapour, as it is demonstrated by the very high mass gain per unit area, 15 times higher than in laboratory air. The corrosion products layer is even thicker (more than 2.5 times) than the one formed in laboratory air with NaCl deposit only. The similarity of the compounds obtained with NaCl deposit in both laboratory and moist airs, residual presence of Cl in the part of the oxide layer closest to the metal/oxide interface, Al enrichment at the metallic substrate surface and absence of an oxygen diffusion area suppose that the corrosion mechanisms are equivalent. Xiong et al. [24] mentioned that the presence of water vapour could lead to the formation of two other harmful compounds [23]: HCl and H_2. Water molecules can react with titanium dioxide, gaseous NaCl (coming from the solid NaCl deposit) and oxygen to form a mixed Na-Ti oxide and gaseous hydrochloric acid (Eq. (9) and (10)). This assumption is supported by the results of thermodynamic calculation presented in Fig. 23, which shows that HCl can be formed in higher quantity than Cl_2. As in laboratory air exposition, the thermodynamic equilibrium reaction involving solid NaCl (Eq. (8)) has a positive standard free enthalpy, while the reaction involving gaseous NaCl (Eq. (9)) has a negative standard free enthalpy (see Table 3).

$$4NaCl_{(s)} + 2H_2O_{(g)} + TiO_{2(s)} \leftrightarrow 2Na_2TiO_{3(s)} + 4HCl_{(g)} \quad (8)$$

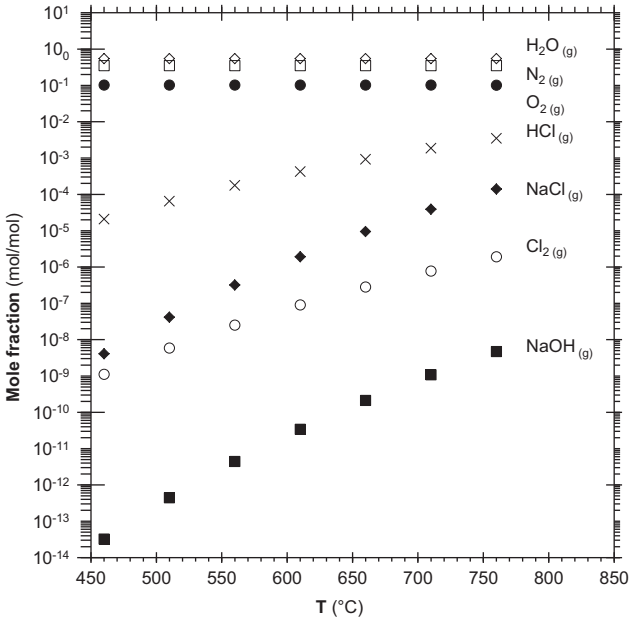

Fig. 23. Evolution of mole fractions of the major gaseous compounds present after the reaction between $TiO_{2(s)}$, $N_{2(g)}$, $O_{2(g)}$, $NaCl_{(s)}$ and in moist air, from 460 °C to 660 °C (determined by FactSage 6.4/ELEM–FactPS–FTPulp database/thermodynamic calculation using equilibrium module considering 1 g of each species).

$$4NaCl_{(g)} + 2H_2O_{(g)} + TiO_{2(s)} \leftrightarrow 2Na_2TiO_{3(s)} + 4HCl_{(g)} \quad (9)$$

As $Na_4Ti_5O_{12}$ phase is equally present after moist air exposition, a corresponding reaction can be written (Eq. (10)), but for the reasons explained above, its standard free enthalpy cannot be calculated.

$$NaCl_{(g)} + 2H_2O_{(g)} + 5TiO_{2(s)} \leftrightarrow Na_4Ti_5O_{12(s)} + 4HCl_{(g)} \quad (10)$$

Analogously to the previous case (reaction between Ti-6Al-4V and NaCl in laboratory air), which involved the migration of gaseous chlorine, this volatile hydrochloric acid could then migrate up to the metal/oxide interface and react with metallic titanium to form gaseous titanium chloride and hydrogen (Eq. (11)).

$$Ti_{(s)} + 4HCl_{(g)} \leftrightarrow TiCl_{4(g)} + 2H_{2(g)} \quad (11)$$

Created hydrogen may then be evacuated out of the reaction area by outward diffusion through pores and cracks or/and diffuse inward to dissolve inside the metallic substrate. Beyond the solubility limit of hydrogen in both α and β phases, hydrogen reacts with titanium to form titanium hydrides. These specific compounds are known to degrade the mechanical properties of Ti and its alloys. In fact, the precipitation of such compounds leads to an embrittlement of the metallic substrate and thus to its more pronounced cracking ability [37–43]. Such cracks occurring near the surface of the metal substrate could then facilitate the inward migration of corrosive gaseous species, contributing to the enhancement of the overall corrosion process.

The titanium chloride can then react with the oxygen and lead to the formation of titanium dioxide and gaseous chlorine, which could also migrate to the metal/oxide interface and keep working the mechanism of active corrosion (Eq. (7)), until the HCl (and by extension the NaCl and H_2O) tank is consumed.

All the steps of the mechanism of active corrosion in $NaCl/H_2O$ environment are summarised in Fig. 24.

In presence of moisture, Deacon equilibrium (Eq. (12)) will also contribute to the mechanism.

$$2H_2O_{(g)} + 2Cl_{2(g)} \leftrightarrow 4HCl_{(g)} + O_{2(g)} \quad (12)$$

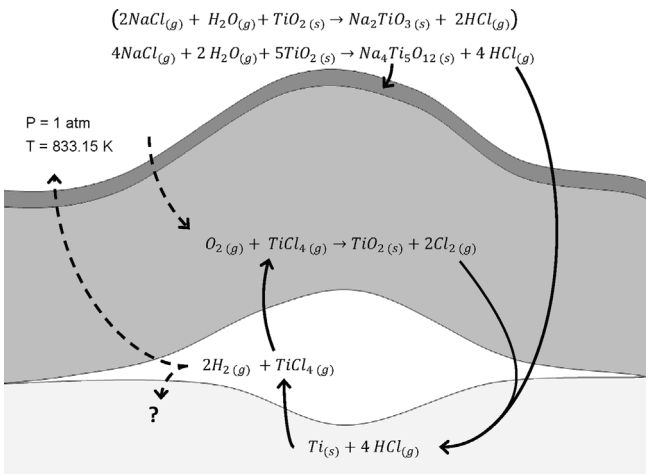

Fig. 24. Diagram of the high temperature cyclic corrosion mechanism of Ti-alloy by NaCl in moist air.

Nevertheless, positive value of standard free enthalpy for Deacon equilibrium provided by thermodynamic predictions in presence of $O_{2(g)}$, $H_2O_{(g)}$, $Cl_{2(g)}$ and $HCl_{(g)}$ at 560 °C indicates that this reaction is favoured in the way of $Cl_{2(g)}$ formation. Thus, the major part of $HCl_{(g)}$ can be converted in $Cl_{2(g)}$, which is known to be more reactive than $HCl_{(g)}$ in the corrosion mechanisms induced by chlorine [32].

The enhancement of the corrosion process is the major evidence of the synergistic effect of NaCl and water vapour on titanium alloys corrosion [23,44]. It can be explained by the conversion of $HCl_{(g)}$ in $Cl_{2(g)}$, via the Deacon equilibrium, which lead to the release of a higher quantity of $Cl_{2(g)}$ than in the previous conditions without moisture. This higher quantity of $Cl_{2(g)}$ can then promote the reaction 6 (Eq. (6)) and enhance the entire mechanism of active corrosion.

Furthermore, the presence of H_2O must be also discussed. Previous works [27,45] showed that the H_2O dissociated mainly at the defects on TiO_2/(110) planes into free H atoms an $OH^{\bullet}$ groups. Their dissolution inside the TiO_2 layer might change the defect chemistry and therefore the transport mechanisms. These considerations might also be possible explanation for the synergistic effect of NaCl and H_2O vapour. A third hypothesis that can be discussed is the presence of an amount of gaseous NaOH, according to thermodynamic predictions (Fig. 23). Knowing that metal hydroxides are precursors to metal chlorides [46,47], the potential impact of this gaseous NaOH on the synergistic effect could be another explanation of the corrosion enhancement phenomenon.

Conclusion

Enhancement of corrosion phenomenon was shown for Ti-6Al-4V alloy with NaCl deposit at high temperature. A synergistic effect was also noticed in presence of water vapour, increasing by a factor of 15 the weight gain per unit area with respect to samples oxidized in dry or moist air at the same temperature. This enhancement is attributed to the presence of gaseous chlorine coming from the NaCl decomposition, leading to the establishment of an active corrosion phenomenon at the metal/oxide interface. The synergistic effect, observed under moist air could be connected to the formation of gaseous HCl or/and NaOH. This large increase in corrosion rate in the presence of NaCl and H_2O is of course of first practical importance since planes and helicopters are used in sea areas. Nevertheless, it should be noticed that the enhanced corrosion mechanism is accompanied by a lack of oxygen enriched area under the corrosion product. Therefore, the consequences of these two phenomena, i.e. oxygen embrittlement under pure oxidation conditions and fast active corrosion under O_2 + NaCl + H_2O conditions, over the mechanical properties of the structural alloys should be evaluated.

Acknowledgements

This work was financially supported by the ICB. The authors would also like to thank Michel VILLASI and Stéphane MATHIEU for fruitful discussions and Frédéric HERBST, Nicolas GEOFFROY and Nathalie ROUDERGUES for technical support.

References

[1] R. Siab, G. Bonnet, J.M. Brossard, J. Balmain, J.-F. Dinhut, Effect of an electrodeposited yttrium containing thin film on the high-temperature oxidation behaviour of TA6V alloy, Appl. Surf. Sci. 253 (2007) 3425–3431, http://dx.doi.org/10.1016/j.apsusc.2006.07.057.
[2] H.L. Du, P.K. Datta, D.B. Lewis, J.S. Burnell-Gray, High-temperature corrosion of Ti and Ti-6Al-4V alloy, Oxid. Met. 45 (1996) 507–527, http://dx.doi.org/10.1007/BF01046849.
[3] H. Guleryuz, H. Cimenoglu, Oxidation of Ti-6Al-4V alloy, J. Alloys Compd. 472 (2009) 241–246, http://dx.doi.org/10.1016/j.jallcom.2008.04.024.
[4] H.L. Du, P.K. Datta, D.B. Lewis, J.S. Burnell-Gray, Air oxidation behaviour of Ti-6Al-4V alloy between 650 and 850°, Corros. Sci. 36 (1994) 631–642, http://dx.doi.org/10.1016/0010-938X(94)90069-8.
[5] H. Guleryuz, H. Cimenoglu, Surface modification of a Ti-6Al-4V alloy by thermal oxidation, Surf. Coat. Technol. 192 (2005) 164–170, http://dx.doi.org/10.1016/j.surfcoat.2004.05.018.
[6] D. Poquillon, C. Armand, J. Huez, Oxidation and oxygen diffusion in Ti-6Al-4V alloy: improving measurements during sims analysis by rotating the sample, Oxid. Met. 79 (2013) 249–259, http://dx.doi.org/10.1007/s11085-013-9360-8.
[7] F. Motte, C. Coddet, P. Sarrazin, M. Azzopardi, J. Besson, A comparative study of the oxidation with water vapor of pure titanium and of Ti-6Al-4V, Oxid. Met. 10 (1976) 113–126, http://dx.doi.org/10.1007/BF00614241.
[8] S.R.J. Saunders, M. Monteiro, F. Rizzo, The oxidation behaviour of metals and alloys at high temperatures in atmospheres containing water vapour: a review, Prog. Mater. Sci. 53 (2008) 775–837, http://dx.doi.org/10.1016/j.pmatsci.2007.11.001.
[9] P. Pérez, On the influence of water vapour on the oxidation behaviour of pure Ti, Corros. Sci. 49 (2007) 1172–1185, http://dx.doi.org/10.1016/j.corsci.2006.06.030.
[10] Y. Wouters, A. Galerie, J.-P. Petit, Thermal oxidation of titanium by water vapour, Solid State Ion. 104 (1997) 89–96, http://dx.doi.org/10.1016/S0167-2738(97)00400-1.
[11] B. Champin, L. Graff, M. Armand, G. Béranger, C. Coddet, Oxydation des alliages de titane au voisinage des températures d'utilisation dans les turbomoteurs, J. Common Met. 69 (1980) 163–183, http://dx.doi.org/10.1016/0022-5088(80)90052-1.
[12] H.J. Grabke, E. Reese, M. Spiegel, The effects of chlorides, hydrogen chloride, and sulfur dioxide in the oxidation of steels below deposits, Corros. Sci. 37 (1995) 1023–1043, http://dx.doi.org/10.1016/0010-938X(95)00011-8.
[13] Y. Kawahara, High temperature corrosion mechanisms and effect of alloying elements for materials used in waste incineration environment, Corros. Sci. 44 (2002) 223–245, http://dx.doi.org/10.1016/S0010-938X(01)00058-0.
[14] P. Kofstad, High Temperature Corrosion, Elsevier Applied Science; Sole distributor in the USA and Canada Elsevier Science Pub. Co, London, New York, NY, USA, 1988.
[15] D.J. Young, High Temperature Oxidation and Corrosion of Metals, 1st ed., Elsevier, Amsterdam; Boston; London, 2008.
[16] G.Y. Lai, High-temperature Corrosion and Materials Applications, ASM International, Materials Park, Ohio, 2007.
[17] C.-C. Tsaur, High temperature oxidation and NaCl-induced accelerated corrosion of hot-dip aluminized 9Cr-1Mo and 310 stainless steel, Texas A&M University, 2005. http://oaktrust.library.tamu.edu/handle/1969.1/1375 (accessed 16.11.15).
[18] P. Dumas, C.S. John, NaCl-induced accelerated oxidation of a titanium alloy, Oxid. Met. 10 (1976) 127–134, http://dx.doi.org/10.1007/BF00614242.
[19] M. Anuwar, R. Jayaganthan, V.K. Tewari, N. Arivazhagan, A study on the hot corrosion behavior of Ti-6Al-4V alloy, Mater. Lett. 61 (2007) 1483–1488, http://dx.doi.org/10.1016/j.matlet.2006.07.058.
[20] J.-D. Béguin, D., Adrian, J.-A. Petit, J.-P. Rivière, C., Vahlas, S. Vaillant, Improvement of salt corrosion resistance of titanium alloys by PVD and CVD coatings, in: Vienna, Austria, (2007) 59–63. http://www.asminternational.org/content/ASM/StoreFiles/05216G_frontmatter.pdf (accessed 03.03.15).
[21] I. Gurrappa, Mechanism of degradation of titanium alloy IMI 834 and its protection under hot corrosion conditions, Oxid. Met. 59 (2003) 321–322, http://dx.doi.org/10.1023/A.1023044111767.
[22] C. Yu, S. Zhu, D. Wei, F. Wang, Oxidation and H_2O/NaCl-induced corrosion behavior of sputtered Ni–Si coatings on Ti6Al4V at 600–650 °C, Surf. Coat. Technol. 201 (2007) 7530–7537, http://dx.doi.org/10.1016/j.surfcoat.2007.02.022.

[23] Y. Shu, F. Wang, W. Wu, Corrosion behavior of ti60 alloy coated with a solid NaCl deposit in O_2 plus water vapor at 500–700 °C, Oxid. Met. 52 (1999) 463–473, http://dx.doi.org/10.1023/A.1018864216554.
[24] Y. Xiong, S. Zhu, F. Wang, Synergistic corrosion behavior of coated Ti60 alloys with NaCl deposit in moist air at elevated temperature, Corros. Sci. 50 (2008) 15–22, http://dx.doi.org/10.1016/j.corsci.2007.06.007.
[25] S. Chevalier, J. Favergeon, French activity on high temperature corrosion in water vapor, (2014) http://alltitles.ebrary.com/Doc?id=10906027 (accessed 03.03.15).
[26] Z.G. Zhang, Y.P. Peng, Y.L. Mao, C.J. Pang, L.Y. Lu, Effect of hot-dip aluminizing on the oxidation resistance of Ti-6Al-4V alloy at high temperatures, Corros. Sci. 55 (2012) 187–193, http://dx.doi.org/10.1016/j.corsci.2011.10.029.
[27] A. Zeller, F. Dettenwanger, M. Schütze, Influence of water vapour on the oxidation behaviour of titanium aluminides, Intermetallics 10 (2002) 59–72, http://dx.doi.org/10.1016/S0966-9795(01)00104-2.
[28] Y. Shu, F. Wang, W. Wu, Corrosion behavior of pure Cr with a solid NaCl deposit in O_2 plus water vapor, Oxid. Met. 54 (2000) 457–471, http://dx.doi.org/10.1023/A.1004690518225.
[29] H.E. Barner, R.V. Scheuerman, Handbook of Thermochemical Data for Compounds and Aqueous Species, Wiley, New York, 1978.
[30] I. Barin, D.O. Knacke, O. Kubaschewski, Thermochemical properties of inorganic substances, in: Thermochem. Prop. Inorg. Subst., Springer Berlin Heidelberg, (1977) 1–861. http://link.springer.com/chapter/10.1007/978-3-662-02293-1_1 (accessed 01.12.15).
[31] A. Ruh, M. Spiegel, Thermodynamic and kinetic consideration on the corrosion of Fe, Ni and Cr beneath a molten KCl–$ZnCl_2$ mixture, Corros. Sci. 48 (2006) 679–695, http://dx.doi.org/10.1016/j.corsci.2005.02.015.
[32] A. Ruh, M. Spiegel, Influence of gas phase composition on the kinetics of chloride melt induced corrosion of pure iron (EU-project OPTICORR), Mater. Corros. 57 (2006) 237–243, http://dx.doi.org/10.1002/maco.200503930.
[33] P.W. Atkins, J. De Paula, Chimie Physique, De Boeck, Bruxelles, 2013.
[34] C.H. McQuarrie, D.A. McQuarrie, P.A. Rock, Chimie générale, De Boeck Université, Bruxelles, 1992.
[35] B.H. Zimm, J.E. Mayer, Vapor pressures, heats of vaporization, and entropies of some alkali halides, J.Chem. Phys. 12 (1944) 362–369, http://dx.doi.org/10.1063/1.1723958.
[36] C.T. Ewing, K.H. Stern, Equilibrium vaporization rates and vapor pressures of solid and liquid sodium chloride, potassium chloride, potassium bromide, cesium iodide, and lithium fluoride, J.Phys. Chem. 78 (1974) 1998–2005, http://dx.doi.org/10.1021/j100613a005.
[37] J.E. Hack, G.R. Leverant, The influence of microstructure on the susceptibility of titanium alloys to internal hydrogen embrittlement, Metall. Trans. A 13 (1982) 1729–1738, http://dx.doi.org/10.1007/BF02647828.
[38] D. Eliezer, E. Tal-Gutelmacher, T. Boellinghaus, Hydrogen embrittlement in hydride-and non hydride-forming systems-microstructural/phase changes and cracking mechanisms, In: Proc. 11th Int. Conf. Fract. Turin Italy, (2005) http://www.gruppofrattura.it/ocs/index.php/ICF/ICF11/paper/view/10870/10199 (accessed 19.03.16).
[39] E. Tal-Gutelmacher, D. Eliezer, The hydrogen embrittlement of titanium-based alloys, JOM 57 (2005) 46–49, http://dx.doi.org/10.1007/s11837-005-0115-0.
[40] E. Tal-Gutelmacher, D. Eliezer, Hydrogen-Assisted degradation of titanium based alloys, Mater. Trans. 45 (2004) 1594–1600, http://dx.doi.org/10.2320/matertrans.45.1594.
[41] G.W. Wille, J.W. Davis, Hydrogen in titanium alloys, McDonnell Douglas Astronautics Co., (1981) http://inis.iaea.org/Search/search.aspx?orig_q=RN:12621440 (accessed March 19, 2016).
[42] N.E. Paton, R.A. Spurling, Hydride habit planes in titanium-aluminum alloys, Metall. Trans. A 7 (1976) 1769–1774, http://dx.doi.org/10.1007/BF02817895.
[43] I.W. Hall, Basal and near- basal hydrides in Ti-5Al-2.5Sn, Metall. Trans. A 9 (1978) 815–820, http://dx.doi.org/10.1007/BF02649790.
[44] L. Liu, Y. Li, F. Wang, Corrosion behavior of metals or alloys with a solid NaCl deposit in wet oxygen at medium temperature, Sci. China Technol. Sci. 55 (2011) 369–376, http://dx.doi.org/10.1007/s11431-011-4675-7.
[45] T. Bredow, K. Jug, Theoretical investigation of water adsorption at rutile and anatase surfaces, Surf. Sci. 327 (1995) 398–408, http://dx.doi.org/10.1016/0039-6028(94)00851-5.
[46] T. Blomberg, P. Makkonen, M. Hiltunen, Role of Alkali Hydroxides in the Fireside Corrosion of Heat Transfer Surfaces, a Practical Approach, Mater Sci. Forum., 461–464 (2004) 883–890 10.4028/www.scientific.net/MSF.461-464.883.
[47] R.W. Bryers, Fireside slagging, fouling, and high-temperature corrosion of heat-transfer surface due to impurities in steam-raising fuels, Prog, Energy Combust. Sci. 22 (1996) 29–120, http://dx.doi.org/10.1016/0360-1285(95)00012-7.